



ARTICLE

YWHAE loss of function causes a rare neurodevelopmental disease with brain abnormalities in human and mouse



ARTICLE INFO

Article history:

Received 10 October 2022

Received in revised form

20 March 2023

Accepted 23 March 2023

Available online 28 March 2023

Keywords:

14-3-3

Brain abnormalities

Miller-Dieker syndrome

Neurodevelopmental disorders

YWHAE

ABSTRACT

Purpose: Miller-Dieker syndrome is caused by a multiple gene deletion, including *PAFAH1B1* and *YWHAE*. Although deletion of *PAFAH1B1* causes lissencephaly unambiguously, deletion of *YWHAE* alone has not clearly been linked to a human disorder.

Methods: Cases with *YWHAE* variants were collected through international data sharing networks. To address the specific impact of *YWHAE* loss of function, we phenotyped a mouse knockout of *Ywhae*.

Results: We report a series of 10 individuals with heterozygous loss-of-function *YWHAE* variants (3 single-nucleotide variants and 7 deletions <1 Mb encompassing *YWHAE* but not *PAFAH1B1*), including 8 new cases and 2 follow-ups, added with 5 cases (copy number variants) from literature review. Although, until now, only 1 intragenic deletion has been described in *YWHAE*, we report 4 new variants specifically in *YWHAE* (3 splice variants and 1 intragenic deletion). The most frequent manifestations are developmental delay, delayed speech, seizures, and brain malformations, including corpus callosum hypoplasia, delayed myelination, and ventricular dilatation. Individuals with variants affecting *YWHAE* alone have milder features than those with larger deletions. Neuroanatomical studies in *Ywhae*^{-/-} mice revealed brain structural defects, including thin cerebral cortex, corpus callosum dysgenesis, and hydrocephalus paralleling those seen in humans.

Conclusion: This study further demonstrates that *YWHAE* loss-of-function variants cause a neurodevelopmental disease with brain abnormalities.

© 2023 The Authors. Published by Elsevier Inc. on behalf of American College of Medical Genetics and Genomics. This is an open access article under the CC BY license (<http://creativecommons.org/licenses/by/4.0/>).

Introduction

Miller-Dieker syndrome (MDS; [MIM 247200]) is a contiguous gene deletion syndrome caused by a microdeletion involving 26 coding genes on human chromosome 17p13.3, including both *PAFAH1B1* and *YWHAE*.¹⁻³ MDS is

characterized by neurodevelopmental delay with classical lissencephaly type 1, microcephaly, brain abnormalities, seizures, and craniofacial abnormalities including a narrow and furrowing forehead, low-set and posteriorly rotated ears, small eyes, upslanting palpebral fissures, epicanthus, a small nose with low nasal bridge, upturned nares, thin upper lip,

The Article Publishing Charge (APC) for this article was paid by Dijon Bourgogne University Hospital.

Anne-Sophie Denommé-Pichon, Stephan C. Collins, and Ange-Line Bruel contributed equally.

Laurence Faivre and Binnaz Yalcin co-directed equally.

*Correspondence and requests for materials should be addressed to Anne-Sophie Denommé-Pichon, Unité Fonctionnelle Innovation en Diagnostic génomique des maladies rares, FHU-TRANSLAD, CHU Dijon Bourgogne, 15 boulevard Maréchal De Lattre de Tassigny, 21070 Dijon CEDEX, France.

Email address: anne-sophie.denomme-pichon@u-bourgogne.fr OR Binnaz Yalcin, INSERM UMR 1231, University of Burgundy, 21000, Dijon, France.

Email address: binnaz.yalcin@inserm.fr

A full list of authors and affiliations appears at the end of the paper.

doi: <https://doi.org/10.1016/j.gim.2023.100835>

1098-3600/© 2023 The Authors. Published by Elsevier Inc. on behalf of American College of Medical Genetics and Genomics. This is an open access article under the CC BY license (<http://creativecommons.org/licenses/by/4.0/>).

cleft palate, and small chin. Additional manifestations include cardiac malformations, urogenital abnormalities, and a failure to thrive. Life span is drastically shortened, with few patients surviving past early childhood.⁴

Smaller deletions or loss-of-function variants involving the proximal *PAFAH1B1* gene alone (formerly named *LIS1* [MIM *601545]) are responsible for isolated lissencephaly (*LIS1*; [MIM 607432]),⁵ making *PAFAH1B1* the main determinant for lissencephaly in patients with MDS. Although the *PAFAH1B1*-associated clinical features are well documented, the specific contribution of the *YWHAE* gene to MDS is understudied. Apart from case report with only one case with a small 12.6-kb intragenic deletion of the *YWHAE* gene presenting brain abnormalities,⁶ the link between *YWHAE* variants alone and human disorders remains understudied, showing a need to build a cohort of individuals with *YWHAE* variants alone.

The *YWHAE* gene (tyrosine 3-monooxygenase/tryptophan 5-monooxygenase activation protein, epsilon isoform [MIM *605066]) encodes the 14-3-3 epsilon protein. 14-3-3ε is highly conserved and implicated in intracellular events involving phosphorylation-dependent switching or protein-protein interactions.⁷ 14-3-3ε is widely expressed throughout the body and at very high levels in various cell types of the central nervous system⁸ where 14-3-3 proteins were originally discovered. 14-3-3ε interacts with doublecortin,⁹ NUDEL, LIS1, and dynein.¹⁰ Its overexpression results in defects in neurite formation.⁹ In humans, duplications involving *YWHAE* and the adjacent genes have been associated to an increased risk of mild developmental delay.¹¹ In vivo, 14-3-3ε is associated with increased motor activity and decreased working memory in mice.^{12,13} 14-3-3ε is involved in corticogenesis and neuronal migration in the CA3 layer of the hippocampus by binding to the NUDEL protein.¹⁰ 14-3-3ε regulates neurogenesis and differentiation of neuronal progenitor cells in the developing mouse brain.¹⁴ The auditory brainstem response shows that mouse *Ywhae* is also involved in hearing and mutant mice have increased minimum detection thresholds at all frequencies.¹⁵

Here, we report and analyze a series of 10 patients, along with 5 cases previously published, with heterozygous loss-of-function *YWHAE* variants collected through international collaborations. The effect of the *YWHAE* loss of function is further investigated through phenotypic characterization of a homozygous knockout mouse model we generated at the Wellcome Sanger Institute (United Kingdom). Together, our results establish a new neurodevelopmental disease caused by loss-of-function *YWHAE* variants both in humans and mice.

Materials and Methods

Human

Patient recruitment

Written informed consent for study participation and publication was obtained by the attending geneticist or the referring physician from the patients' legal guardians.

Collection of cases: Data sharing networks

Cases were collected through data sharing networks. The cases included in this study were gathered through GeneMatcher,¹⁶ the Decipher database, the ITHACA European Reference Network, the French AnDDI-Rares network, and through personal correspondence. We included cases with single-nucleotide variants (SNVs) in *YWHAE* or deletions of less than 1 Mb encompassing *YWHAE* but not *PAFAH1B1*. We chose not to include cases with *PAFAH1B1* deletion to increase detection power of phenotypes specific to *YWHAE*.

Clinical characteristics were assessed through a standardized phenotyping sheet and included data on magnetic resonance imaging-based neuroimaging.

Genetic testing and targeted RNA study

In all patients, variants and deletions disrupting *YWHAE* were detected by either chromosomal microarray analysis or next-generation sequencing. For a description of chromosomal microarray analysis and next-generation sequencing methodology, see the [Supplemental Methods](#). All variants reported in this study refer to *YWHAE* transcript NM_006761.5. Genomic coordinates refer to the GRCh37 human reference genome. SNVs were classified using American College of Medical Genetics and Genomics guidelines.¹⁷

For the cases with SNVs, we set out to assess the variant's impact on splicing. Cases 2 and 3 (2 monozygotic twins carrying the same variant) underwent targeted RNA study. Total RNA was extracted from whole blood collected in a PAXgene tube (Preanalytics GmbH, Hombrechtikon, Switzerland) using the PAXgene Blood RNA kit (Preanalytics GmbH, Hombrechtikon, Switzerland) following the standard protocol. Complementary DNA was obtained using the QuantiTect Reverse Transcription kit (Qiagen GmbH, Hilden, Germany). RNA from case 1 was not available and has not been studied. The conditions for reverse transcription polymerase chain reaction (RT-PCR) are detailed in the [Supplemental Methods](#).

Phenotypic features comparison

Patients for whom a specific feature information was missing were not included in that feature's statistic; hence, the group sizes differ between features. We used the Fenton preterm growth charts with term-corrected age to assess birth measurements and World Health Organization growth charts from 0 to 5 years and from 1 to 18 years to assess measurements after birth.

Mouse

Generation of *Ywhae* knockout mouse model

The knockout mouse model was generated by homologous recombination using the knockout-first allele method, producing the *Ywhae*^{tm1e(EUCOMM)Wtsi} knockout allele. The *Ywhae* gene was targeted in C57BL/6N embryonic stem cells with a conditional-ready cassette (clone EPD0200_5_G01) as described previously.¹⁸ Germline

transmission was confirmed by a series of genotyping and quantitative polymerase chain reaction analyses using the standard International Mouse Phenotyping Consortium quality control validation strategy, with the results found here (<https://www.mousephenotype.org/data/genes/MGI:894689>). Mice derived from heterozygous (Het) intercross were genotyped for the *Ywhae*^{tm1e} allele by polymerase chain reaction carried out as previously described.¹⁹ On a C57BL/6N background, Het mice were subviable: 20 Het mice of 192 offspring were obtained from Het × wild-type (WT) matings at weaning.¹⁵ The line was then crossed with 129S5/SvEvBrd/Wtsi to improve viability. Mice were produced from Het × Het matings to give segregating litters that included homozygous knockout (Hom), Het, and WT as littermate controls. A subset of these mice was used in neuroanatomical characterization.

Mouse whole-body phenotyping studies

The *Ywhae*^{tm1e(EUCOMM)Wtsi} knockout mice were phenotyped for whole-body traits by the Mouse Genetics Project pipeline at the Wellcome Sanger Institute, United Kingdom (for details, see the [Supplemental Methods](#)). In brief, mice of both sexes were weighed between 4 and 16 weeks of age and assessed at 9 weeks for gross behavioral abnormalities (modified SHIRPA²⁰) and dysmorphology using standardized procedures. For each test, *Ywhae*^{tm1e/tm1e} were tested alongside littermate *Ywhae*^{+/+} controls through the pipeline, which included tests for indirect calorimetry, body composition, x-ray morphology, blood chemistry, and hematology ($n = 6$ for WT and $n = 7$ for Hom mice).

Comprehensive neuroanatomical studies

Neuroanatomical studies were carried out using 3 *Ywhae*^{tm1e/tm1e} male and 5 WT male mice (2 littermates and 3 mice from the same mixed background) at 16 weeks of age. Mice were anesthetized with ketamine (100 mg/kg, intraperitoneal) and xylazine (10 mg/kg, intraperitoneal). Brains were dissected and fixed in 4% neutral buffered formalin for 48 hours, then transferred to 70% ethanol. Samples were embedded in paraffin using an automated embedding machine (Sakura Tissue-Tek VIP) and cut at a thickness of 5 μm with a sliding microtome (Leica RM 2145) to obtain coronal brain region at Bregma +0.98 mm according to the Allen Mouse Brain Atlas. The sections were then stained with 0.1% Luxol Fast Blue (Solvent Blue 38; Sigma-Aldrich) and 0.1% cresyl violet acetate (Sigma-Aldrich) and scanned using Nanozoomer 2.0HT, C9600 series at 20× resolution, as previously described.²¹

Image analysis

Twenty-two brain parameters, made up of area and length measurements, were taken blind to the genotype. Using in-house ImageJ plugins, an image analysis pipeline was used to standardize measurements. Each image was quality controlled for the accuracy of sectioning relative to the reference Allen Mouse Brain Atlas and controlled for asymmetries and histological artifacts.²² At Bregma +0.98

mm, the brain structures assessed were as follows: (1) the total brain area, (2) the lateral ventricles, (3) the cingulate cortex, (4) the genu of the corpus callosum, (5) the caudate putamen, (6) the anterior commissure, (7) the piriform cortex, (8) the primary motor cortex, and (9) the secondary somatosensory cortex. All samples were also systematically assessed for cellular ectopia (misplaced neurons). Mouse neuroanatomical data were analyzed using a two-tailed *t* test assuming equal variance.

Mouse embryogenesis and high-resolution episcopic microscopy

To study mouse embryogenesis, we generated Het × Het timed matings on a mixed C57BL/6N and 129S5/SvEvBrd/Wtsi genetic background. We produced 44 embryos at embryonic day 14.5 (E14.5), of which 3 Hom and 3 WT were sent to the Deciphering the Mechanisms of Developmental Disorders consortium (<https://dmdd.org.uk>) for high-resolution episcopic microscopy (HREM) processing. The detailed protocol has been published previously.²³ Briefly, 14.5-day embryos were embedded in a hard plastic resin, enabling thin sectioning (1 μm). This resin contains a fluorescent dye, which allows contrast between the tissue and the bright background of the plastic. By sequentially imaging the block face during the sectioning process, a comprehensive stack of accurately aligned images was acquired, documenting the 3-dimensional structure of the sample. We then carried out a comprehensive assessment of brain morphometrics by adapting our 2-dimensional histology protocol used in adult mice to 3-dimensional brain stacks.²⁴

Results

We present a series of 8 new and 2 follow-ups, along with 5 other previously published cases from a literature review.^{6,25-30} In total, 15 patients (7 males, 7 females, and 1 unknown) from 14 unrelated families with heterozygous loss-of-function *YWHAE* variants were collected: 3 splice site variants (cases 1-3), 2 intragenic deletions (cases 10 and 14), and 10 large deletions (<1 Mb), encompassing *YWHAE* but not *PAHAFAB1* (cases 4-9, 11-13, and 15) ([Figure 1A](#) and [B](#)).

Variants occurred de novo (10 of 12) or were inherited from a symptomatic parent (1 of 12) or from a healthy father with paternal mosaicism (1 of 12). In 3 of 15 cases, inheritance is not known.

The c.715+1G>T variant present in cases 2 and 3 affects the donor splice site of intron 5 of *YWHAE*. Analysis of RT-PCR products from cases 2 and 3 by gel electrophoresis showed 2 bands corresponding to 2 RNAs of different sizes ([Figure 1C](#)). The study of variant impact on pre-messenger RNA splicing using targeted complementary DNA sequencing showed the skipping of exon 5 (NM_006761.4:r.579_715del) in a heterozygous state, with 40,920 of 87,290 reads in case 2 and 10,437 of 22,352 reads

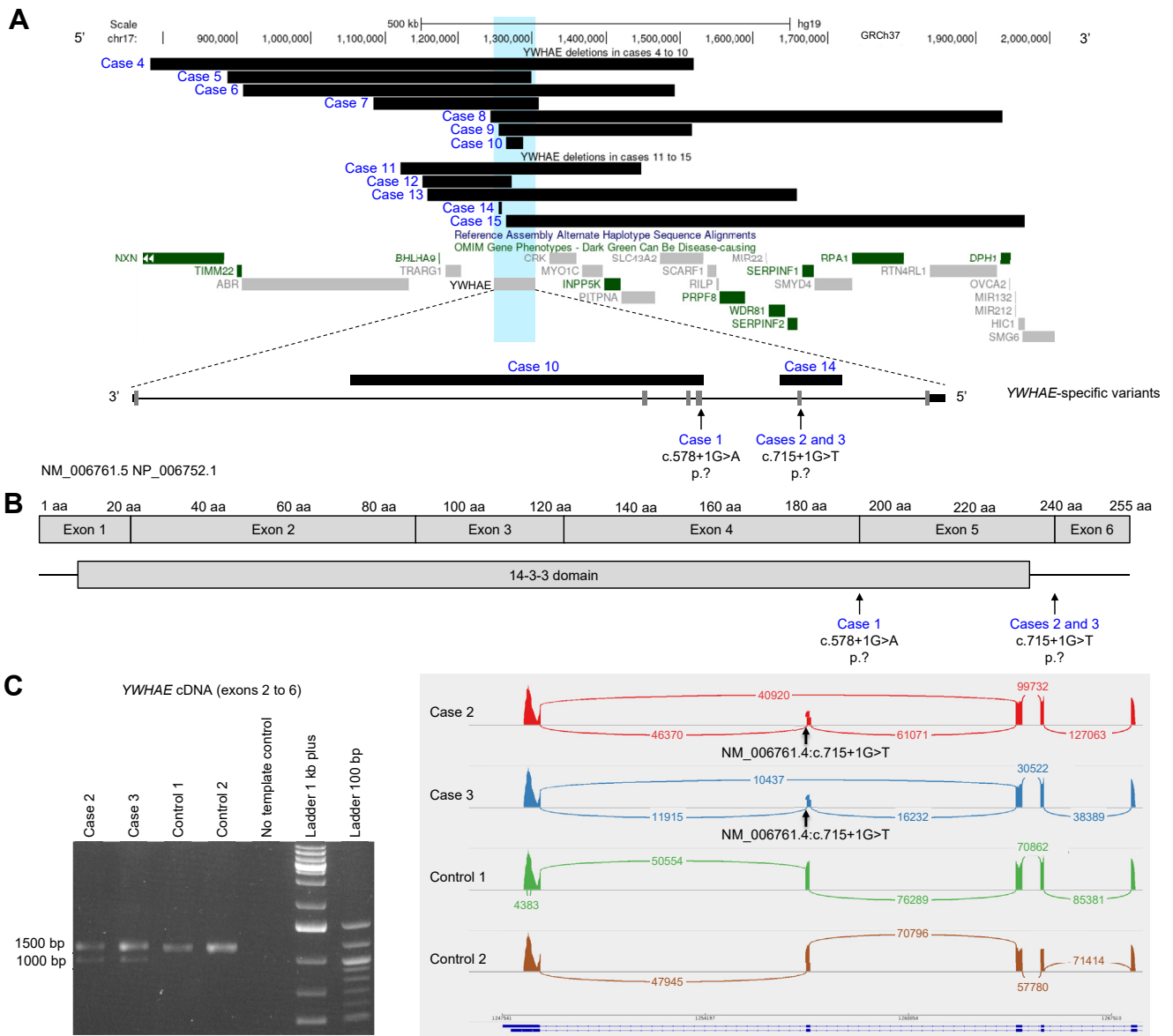


Figure 1 *YWHAE* variants reported in this study and analysis of splice site variant. **A.** *YWHAE* variants at the gene level shown using the UCSC Genome Browser tool³⁸ (GRCh37 assembly): single-nucleotide variants in cases 1, 2, and 3 and deletions <1 Mb encompassing *YWHAE* in cases 4 to 15. Five cases present with variants specifically in *YWHAE*, including 3 splice variants and 2 intragenic deletions. Genes highlighted in green are reported in OMIM to be disease causing, whereas genes in gray are not disease causing. *YWHAE* location is depicted in cyan. Coding exonic regions are depicted with gray shading. **B.** Variants in cases 1, 2, and 3 are positioned at the protein level (NM_006761.5 NP_006752.1). Coding exon regions and 14-3-3 domain are depicted with gray shading. **C.** Left panel: analysis by gel electrophoresis of exons 2 to 6 RT-PCR products from cases 2 and 3 showing 2 bands corresponding to 2 RNAs of different sizes. Right panel: study of variant impact on pre-messenger RNA splicing using targeted RNA deep sequencing showing heterozygous exon 5 skipping. *cDNA*, complementary DNA; *RT-PCR*, reverse transcription polymerase chain reaction.

in case 3, leading to the deletion of 127 nucleotides, predicted to cause a frameshift and create a premature stop codon p.(Leu194*) (Figure 1C). These additional results confirm that the c.715+1G>T variant results in an aberrant splicing of the *YWHAE* gene.

The main clinical features are summarized in Table 1 and fully detailed in Table 2. The mean age at the time of the last evaluation was 10 years (from 19 weeks of gestation to 39 years old). There was no apparent difference in severity between males and females. Almost all patients had

developmental delay (13 of 14) with impaired speech or language (11 of 11). The age of the first sentences ranged from 2 years 6 months to 3 years 4 months (mean of 2 years 7 months). Motor delay was less common: 3 of 10 started to walk after 18 months (from before 12 to 30 months), 3 of 8 had impaired gait, and 4 of 7 impaired hand skills such as dyspraxia (2 of 7). When present and evaluable, intellectual disability (ID) (6 of 13) was mild to severe, and, interestingly, variants strictly within *YWHAE* were associated with ID in only 1 case (case 1), presenting with mild ID.

Table 1 Comparative summary of clinical features between individuals with variants in *YWHAE* only, individuals with variants in *YWHAE* and other genes, and *Ywhae*^{tm1e/tm1e} mice, from this study and a literature review^{9,10,12-15}

Clinical Features	Variants in <i>YWHAE</i> Only	Variants in <i>YWHAE</i> and Other Genes	Total	<i>Ywhae</i> ^{+/-} Mice Literature	<i>Ywhae</i> ^{-/-} Mice Literature	<i>Ywhae</i> ^{-/-} Mice This Study
Developmental delay	5/5	8/9	13/14	Not available	+ ¹³	Not available
Intellectual disability	1/5 (mild)	5/8 (mild to severe)	6/13	Not available	Not available	Not available
Memory impairment	Not available	Not available	Not available	+ ¹²	+ ¹³	Not available
Delayed or impaired speech	5/5	6/6	11/11	Not available	Not available	Not available
Hypotonia	4/4	3/8	7/12	+ ¹³	++ ¹³	Not available
Seizures	4/5	4/8	8/13	Not available	Not available	Not available
Behavioral disorder	3/4	3/8	6/12	+ Hyperactivity ^{12,13}	++ ¹³	+
Anxiety	2/4	1/8	3/12	+/- ^{12,13}	Not available	Not available
Brain malformations	4/4	4/8	8/12	+ ¹⁰	++ ¹⁰	+
Corpus callosum hypoplasia	3/4	2/7	5/11	Not available	Not available	++
Ventricular dilatation	2/4	1/7	3/11	Not available	Not available	+++
Poor myelination	2/4	1/7	3/11	Not available	Not available	Not available
Cortical hypoplasia	0/4	2/7	2/11	+ ¹⁰	++ ¹⁰	++
Hippocampal defects	Not reported	Not reported	Not reported	+ ¹⁰	++ ¹⁰	Not available
Growth retardation	0/4	4/7	4/11	+/- ^{12,13}	++ ^{13,15} (see also Ref. 10)	+
Craniofacial features	3/5	9/10	12/15	Not available	+ (shortened skull ¹⁵)	+ (shortened skull)
Hearing impairment	Not reported	Not reported	Not reported	Not available	Moderate ¹⁵	Not available

The severity of the signs increases with the number of “+” symbols. The symbol +/- indicates inconsistent results between mouse studies, which we briefly comment on here: for the assessment of anxiety, Ikeda et al¹² used the elevated plus maze, whereas Wachi et al¹³ the open field test; for growth retardation, the effect of the Ikeda et al’s study was mild¹²; therefore, it could be a false positive. To facilitate the interpretation of the murine findings, we also provide the full nomenclature of the models used in the literature review: for Toyo-oka et al,¹⁰ allele designation *Ywhae*^{tm1Awb}, genetic background 129S6/SvEvTac × NIH Black Swiss¹⁰; for Ikeda et al¹² same as Toyo-oka et al¹⁰; for Cornell et al and Toyo-oka et al,¹⁴ allele designation *Ywhae*^{tm2.1Awb}, genetic background 129S6/SvEvTac × C57BL/6J^{9,14}; for Wachi et al,¹³ allele designation *Ywhae*^{tm1Awb}, genetic background 129S6/SvEvTac¹³; and for Ingham et al¹⁵ and this study, allele designation *Ywhae*^{tm1e(EUCOMM)Wtsi}, genetic background C57BL/6N × 129S5/SvEvBrd/Wtsi.¹⁵

Table 2 Full description of the *YWHAE* phenotypic and molecular findings in the study's cohort

Cases	1	2	3	4	5	6	7	8	9	10	11	12	13	14	15
Publication	This study	This study	This study	PMID 32323081 (Romano et al ⁽²⁵⁾) Follow-up	PMID 19635726 (Mignon-Ravix et al ⁽²⁶⁾) Follow-up	This study	This study	This study	This study	This study	PMID 20452996 (Bruno et al. ³⁰ patient 3)	PMID 19584063 (Nagamani et al. ³⁰ patient 1)	PMID 20599530 (Schiff et al. ²⁸ patient D)	PMID 28542865 (Noor et al ⁽⁷⁾)	PMID 29458882 (Chen et al ⁽⁷⁾)
Variant	NM_006761.5:c.578+1G>A p.?	NM_006761.5:c.715+1G>T p.(Leu194*)	NM_006761.5:c.715+1G>T p.(Leu194*)	arr[GRCh37] 17p13.3(783542_1518383)x1	arr[GRCh37] 17p13.3(887704_1298810)x1	arr[GRCh37] 17p13.3(908480_1492475)x1.ish	arr[GRCh37] 17p13.3(1084016_1308796)x1dn	arr[GRCh37] 17p13.3(1244153_1935766)x1	arr[GRCh37] 17p13.3(1254875_1516480)x1dn	arr[GRCh37] 17p13.3(1264229_1288574)x1	arr[GRCh37] 17p13.3(1120324_1447883)x1dn	arr[GRCh37] 17p13.3(1151382_1272389)x1dn	arr[GRCh37] 17p13.3(1158449_1658551)x1	arr[GRCh37] 17p13.3(1254694_1258917)x1dn	arr[GRCh37] 17p13.3(1264243_1965733)x1dn
Deletion (included genes)	NA (<i>YWHAE</i>)	NA (<i>YWHAE</i>)	NA (<i>YWHAE</i>)	735 kb (<i>MRM3</i> , <i>NXN</i> , <i>TIMM22</i> , <i>ABR</i> , <i>BHLHA9</i> , <i>TRARG1</i> , <i>YWHAE</i> , <i>CRK</i> , <i>MYO1C</i> , <i>INPP5K</i> , <i>PITPNA-AS1</i> , <i>PITPNA</i>)	411 kb (<i>TIMM22</i> , <i>ABR</i> , <i>BHLHA9</i> , <i>TRARG1</i> , <i>YWHAE</i>)	584 kb (<i>ABR</i> , <i>BHLHA9</i> , <i>TRARG1</i> , <i>YWHAE</i> , <i>CRK</i> , <i>MYO5C</i> , <i>INPP5K</i> , <i>PITPNA-AS1</i> , <i>PITPNA</i> , <i>SLC43A2</i>)	224 kb (<i>ABR</i> , <i>BHLHA9</i> , <i>TRARG1</i> , <i>YWHAE</i>)	692 kb (<i>YWHAE</i> , <i>CRK</i> , <i>MYO1C</i> , <i>INPP5K</i> , <i>PITPNA-AS1</i> , <i>PITPNA</i> , <i>SLC43A2</i> , <i>SCARF1</i> , <i>RILP</i> , <i>PRPF8</i> , <i>TLCD2</i> , <i>WDR81</i> , <i>SERPINF2</i> , <i>SMYD4</i> , <i>RPA1</i> , <i>RTN4RL1</i> , <i>OPH1</i>)	262 kb (<i>YWHAE</i> , <i>CRK</i> , <i>MYO1C</i> , <i>INPP5K</i> , <i>PITPNA-AS1</i> , <i>PITPNA</i> , <i>SLC43A2</i> , <i>RN75L105P</i>)	24 kb (<i>YWHAE</i> , exons 2 to 4)	328 kb (<i>ABR</i> , <i>BHLHA9</i> , <i>TRARG1</i> , <i>YWHAE</i> , <i>CRK</i> , <i>INPP5K</i> , <i>MYO1C</i> , <i>PITPNA</i> , <i>PITPNA-AS1</i> , <i>TRARG1</i> , <i>YWHAE</i>)	121 kb (<i>BHLHA9</i> , <i>TRARG1</i> , <i>YWHAE</i>)	500 kb (<i>BHLHA9</i> , <i>TRARG1</i> , <i>YWHAE</i> , <i>CRK</i> , <i>MYO1C</i> , <i>INPP5K</i> , <i>PITPNA</i> , <i>PITPNA-AS1</i> , <i>TRARG1</i> , <i>YWHAE</i>)	12.6 kb (<i>YWHAE</i> , exon 5)	701 kb (<i>YWHAE</i> , <i>CRK</i> , <i>MYO1C</i> , <i>INPP5K</i> , <i>PITPNA-AS1</i> , <i>PITPNA</i> , <i>SLC43A2</i> , <i>SCARF1</i> , <i>RILP</i> , <i>PRPF8</i> , <i>TLCD2</i> , <i>WDR81</i> , <i>SERPINF2</i> , <i>SMYD4</i> , <i>RPA1</i>)
Inheritance	De novo	De novo	De novo	Inherited from healthy father (paternal mosaicism)	NA (father not available)	De novo	De novo	NA	De novo	Inherited from affected father (minor phenotype)	De novo	De novo	NA	De novo	De novo
Classification	Pathogenic (PV51, PS2, PM2)	Pathogenic (PV51, PS2, PM2)	Pathogenic (PV51, PS2, PM2)	Pathogenic	Pathogenic	Pathogenic	Pathogenic	Pathogenic	Pathogenic	Pathogenic	Pathogenic	Pathogenic	Pathogenic	Pathogenic	Pathogenic
Technology of variant detection	Multigene panel (1637 genes)	Exome sequencing	Exome sequencing	CMA	CMA	CMA	CMA	CMA	CMA	CMA	CMA	CMA	CMA	CMA	CMA
Sex	Male	Female	Female	Female	Male	Female	Female	Female	Male	Female	Male	Male	Male	Male	NA
Gestational age	38 + 2 wg	30 wg	30 wg	39 + 2 wg	41 + 5 wg	38 wg	41 + 6 wg	NA	39 + 5 wg	38 wg	36 + 4 wg	NA	37 wg	At term	19 wg
Length at birth	49 cm (50th p.)	41.5 cm (90th p.)	41 cm (90-90th p.)	46 cm (3-10th p.)	49.5 cm (10th p.)	NA	51 cm (10-50th p.)	NA	48 cm (10th p.)	47.5 cm (10-50th p.)	46 cm (10-50th p.)	NA	44 cm (3rd p.)	NA	NA
Weight at birth	2820 g (10-50th p.)	1520 g (50-90th p.)	1695 g (90th p.)	2550 g (3-10th p.)	3260 g (10th p.)	2752 g (10-50th p.)	3340 g (10-50th p.)	NA	2878 g (10th p.)	3025 g (50th p.)	2270 (10th p.)	3180 g	2400 g (10th p.)	3700 g (50-90th p.)	268 g
Head circumference at birth	33.5 cm (50th p.)	30 cm (97th p.)	30 cm (97th p.)	33 cm (10th p.)	38 cm (95th p.)	NA	NA	NA	35 cm (50th p.)	32.5 cm (10-50th p.)	Normal	NA	33.5 cm (50th p.)	NA	NA
Prenatal features	Normal	Normal	Normal	IUGR, oligohydramnios	Normal	Polyhydramnios	Normal	Normal	SARS-CoV-2 infection (first trimester)	Nuchal translucency	NA	No	NA	NA	NA
Age at last evaluation	3 y 10 mo	10 y 4 mo	10 y 4 mo	4 y	13 y	14 y	14 y	39 y	11.5 mo	5 y 3 mo	NA	13 y	4 y	8 y 4 mo	19 wg
Weight	17.5 kg (+0.5 SD)	24 kg (-2 SD)	24 kg (-2 SD)	NA	36 kg (-1 SD)	25.9 kg (-3 SD)	NA	NA	10.33 kg (+0.5 SD)	26 kg (+2 SD)	NA	47 kg (M)	12.6 kg (-2.3 SD)	NA	268 g
Height	101 cm (M)	128 cm (-1.7 SD)	128 cm (-1.7 SD)	NA	132 cm (-2.5 SD)	124.3 cm (-5.5 SD)	NA	NA	77 cm (+1 SD)	115 cm (+1 SD)	NA	145.4 cm (-1.3 SD)	93 cm (-2.5 SD)	NA	NA
Head circumference	53 cm (+1.6 SD)	52.7 cm at 8 y 10 mo (+0.5 SD)	52 cm at 8 y 10 mo (M)	NA	58.5 cm (+3 SD)	51.6 cm (-2 SD)	NA	57.3 cm (+1.5 SD)	48 cm (+1 SD)	52 cm (+1 SD)	NA	49.7 cm (-3 SD)	51.5 cm (+0.5 SD)	NA	NA
Growth retardation DD	No	No	No	NA	Yes	Yes	Yes	No	No	No	Yes	No	Yes	NA	NA
ID	Mild	No	No	Mild	Mild to moderate	No	Moderate to severe	Mild	NA	No	No	Mild to moderate	No	No	NA
Walking age	18 mo	30 mo	30 mo	18 mo	30 mo	12-13 mo	<12 mo	NA	NA	NA	16.5 mo	NA	12 mo	Normal	NA
Gait	Impaired	Normal	Normal	NA	Impaired	Normal	Impaired	Normal	NA	NA	NA	NA	Normal	NA	NA
Hand skills	Impaired (difficulties in fine motor)	Dyspraxia	Dyspraxia	NA	Normal	Normal	NA	NA	Normal	Impaired	NA	NA	NA	NA	NA

(continued)

Table 2 Continued

Cases	1	2	3	4	5	6	7	8	9	10	11	12	13	14	15
Age at first sentence	2.5 y	2.5 y	2.5 y	MA	MA	2-3 y	>3 y	MA	NA	NA	NA	NA	First word at 40 mo	NA	NA
Speech/language development or troubles	Make sentence, difficulties in articulation	Dysphasia	Dysphasia	Impaired	Impaired, reading acquired	Impaired, some words at 13 y	Impaired	Impaired, poor articulation, nasal voice	NA	NA	NA	NA	Delayed	Dysgraphia	NA
Seizures	Generalized febrile seizure	Tonic-clonic, multilaterally absences	No	Daily seizures, brisk episodes of head, limbs flexion on trunk, awakening and crying	No	No	Tonic-clonic, myoclonic and absence seizures	Only one epileptic seizure	Infantile spasms	Eye revulsions	NA	No	No	Myoclonic	NA
Age at first seizure	16 mo (only 1 seizure)	9 y	MA	5 mo	NA	NA	1 y	MA	4.5 mo	NA	NA	NA	NA	2.5 y	NA
Seizure treatment	No	Levetiracetam (no effective) and valproate (effective)	MA	Vigabatrin followed by 1 ACTH cycle	NA	NA	Drug resistant, anticonvulsants and spinal cord stimulator	No	Vigabatrin, prednisolone and ketogenic diet	NA	NA	NA	NA	Ethosuximide	NA
EEG	Normal	Discontinuous pattern, abundant theta frequencies, bilateral temporal positive spikes	MA	Strong diffuse multifocal paroxysmal activity (spike-and-wave and polyspike-and-wave)	NA	NA	Disorganized sleep and wake patterns, rather diffuse abnormalities during sleep	Irregular spike-wave complexes on the right side	Infantile spasms, wake and sleep differentiated at the diagnosis of infantile spasms	NA	NA	NA	NA	NA	NA
Brain MRI or CT	Pituitary hypoplasia, small unilateral arachnoid cyst	Intraventricular hemorrhage, germinalytic cyst, ventricular dilatation, absence of the olfactory bulbs, hypoplasia of the cerebral white matter, enlarged thin corpus callosum, enlarged Virchow-Robin spaces, cerebellar vermiform hypoplasia	Ventricular dilatation, cyst of the septum pellucidum and the cavum vergae, thin corpus callosum and enlarged white matter, Virchow-Robin spaces, delayed myelination, cerebellar vermiform hypoplasia, absence of the olfactory bulbs	Slight widening of anterior portion of left Sylvian fissure, reduced volume of callosum, inferior frontal parenchyma with widening of ipsilateral superficial liquor spaces, poor myelination	Nodular heterotropias, hypoplasia of the corpus callosum, polymicrogyria, abnormal bulging of the brainstem	Normal	Normal	NA	Normal (thalamic restriction: vigabatrin?)	Normal	Not performed	Thinning of corpus callosum and frontal cortex	Cobloombatous cyst near right optic nerve, normal aspect of the white matter and enlarged Virchow-Robin spaces	Chiari I, thin corpus callosum, thin cavum septum pellucidum and cavum vergae	NA
Behavioral disorders	No	Anxiety, skin scratching, ADHD, short attention span	MA	MA	Yes	No	Low frustration tolerance	Anxiety, obsessive-compulsive behavior, self-injury, always looking food, abnormal temper tantrums, skin scratching	No	ADHD	No	No	No	NA	NA
Neuromuscular abnormalities	Hypotonia	Hypotonia in early childhood	Hypotonia in early childhood	MA	Normal	Occasional tremors	Normal	Intentional tremors	Hypotonia	Hypotonia	Hypotonia	Mild hypotonia	No	NA	NA
Eye abnormalities	Nystagmus, strabismus, mild hypoplasia of optic nerve	No	No	No	Strabismus, nystagmus, hypertelorism	Mild hypertelorism	No	No	No	No	Iris coloboma	No	Hypertelorism, right microomea, ptosis, bilateral chorioretinal and lens coloboma	No	NA
Epicentrus	No	No	No	No	Yes	Yes	No	Yes	No	Yes	No	Yes	No	No	Yes

(continued)

Table 2 Continued

Cases	1	2	3	4	5	6	7	8	9	10	11	12	13	14	15
Downslanting palpebral fissures	No	No	No	No	Yes	No	No	No	No	Yes	Yes	Yes	Yes	No	No
Ear abnormalities	No	No	No	Folded left ear helix	Small, low-set, and posteriorly rotated, thick and irregular helix	No	No	No	No	No	Low-set ears, cupped	Low-set ears, large auricles	No	Low-set ears	Low-set ears
Other craniofacial features	Sparse eyebrows	No	No	Slight periorbital edema, thin upper and thick lower lip, arched eyebrows, flat nasal root, bulbous nasal tip	Prominent forehead, pronounced cupid bow, macrocephaly, anteverted nares	NA	Dark circles around the eyes	Large head	No	Thin upper lip	Broad face, normal forehead, laterally extended eyebrows, broad nasal tip and base, micrognathia, thick and everted upper lip	Prominent forehead, tall vertex, retrognathia, thin upper lip	Large face, short nose, everted lower lip, pointed chin	Prominent forehead and occiput, bitemporal narrowing, furrowed brow, broad nasal root, anteverted nostrils, micrognathia	Microcephaly, broad nasal bridge, anteverted nostrils, micrognathia
Skeletal defects	Hyperlaxity	Clinodactyly of the fourth and fifth fingers	Clinodactyly of the fifth fingers	Clinodactyly of the fifth fingers	No	No	Camptodactyly of the fifth fingers, familial syndactyly of second and third toes	Genu recurvatum, large hands and feet	No	No	No	Arthrogryposis of upper limbs	No	NA	NA
Gastrointestinal features	No	Abdominal pain, tympanites, diarrhea, cow's milk protein intolerance	Abdominal pain, tympanites, diarrhea, cow's milk protein intolerance	No	No	Feeding difficulties in early infancy, swallow studies showed laryngeal penetration	No	No	Constipation	No	Neonatal feeding difficulties	No	No	NA	NA
Urogenital and kidney abnormalities	No	Enuresis nocturna	No	No	Unilateral cryptorchidism	No	No	No	No	No	NA	Anteriorly placed anus, VUR, hydronephrosis	No	NA	NA
Cardiac anomalies	No	No	Valvular pulmonary stenosis, VSD spontaneously resolved	No	No	No	No	No	Ventricular extrasystoles	NA	NA	NA	No	NA	NA
Skin abnormalities	No	Congenital nevus	No	No	No	No	Five small cafe-au-lait spots	Scratching and skin papules	No	No	NA	No	No	NA	NA
Endocrine dysfunction	No	No	No	No	Thyrotropic and corticotropic deficit substituted since age 13 y	GH deficiency treated by GH supplementation since age 9 y	NA	Diabetes mellitus, high triglycerides, GH deficiency treated by GH during childhood	No	NA	NA	NA	No	NA	NA
Other		Anosmia, enamel brittleness	Anosmia, abnormal enamel					Neonatal hyperbilirubinemia with exchange transfusion, fat accumulation hips, daytime sleepiness, low neutrophils	No		No recurrent infections	No	No	Learning difficulties related to mathematics	

ACTH, adrenocorticotropic hormone; *ADHD*, attention-deficit/hyperactivity disorder; *CMA*, chromosomal microarray analysis; *CT*, computed tomography, *EEG*, electroencephalogram; *GH*, growth hormone; *IUGR*, intrauterine growth retardation; *MRI*, magnetic resonance imaging; *NA*, not available or not applicable; *p*, percentile; *SD*, standard deviation; *VSD*, ventricular septal defect; *VUR*, vesicoureteral reflux; *wg*, weeks of gestation.

Behavioral disorders were frequent (6 of 12), and some patients were reported with attention-deficit/hyperactivity disorder (3 of 12) and anxiety (3 of 12). Growth retardation was observed only in patients with a deletion encompassing more than just *YWHAE* (4 of 11). Hypotonia seemed to be frequent (7 of 12), accompanied by feeding difficulties in 2 patients. Tremor was reported (2 of 11). Seizures were frequent (8 of 13) with a mean age of onset of 2.4 years (from 4.5 months to 9 years). Seizures were tonic-clonic, myoclonic, spasms, absence, or febrile. Some individuals had several types of seizure, and 2 of 8 patients presented with multiday seizures. Brain malformations were common (8 of 12) (Figure 2A) and included signs of altered myelination (ventricular dilation [3 of 8], corpus callosum hypoplasia [5 of 8], poor myelination [3 of 8]), cysts (subependymal germinolytic, septum pellucidum, cavum vergae, arachnoid, and near optic nerve) (4 of 8), cerebellar hypoplasia (3 of 8), enlarged Virchow-Robin spaces (3 of 8), thinning of the frontal cortex (2 of 8), absence of the olfactory bulbs (2 of 8), Chiari malformation type 1 (1 of 8), intraventricular hemorrhage (1 of 8), pituitary hypoplasia (1 of 8), polymicrogyria (1 of 8), and nodular heterotopias (1 of 8). Craniofacial features were observed in 12 of 15 patients, among which 3 of 5 with variants strictly within *YWHAE*, presenting milder and nonspecific dysmorphic features (Figure 2B). Skeletal defects were observed in 7 of 13 patients, with clinodactyly or camptodactyly of the fourth or the fifth fingers in 4 of 7 individuals. Although individuals did not have their hearing tested, no impairments were reported.

We next thought to characterize and evaluate datasets from a *Ywhae*^{tm1e(EUCOMM)Wtsi} knockout mouse model with a focus on the most frequent clinical components of the human disorder. Results of knockout mice from this study and a literature review are summarized in Table 1.^{9,10,12-15} According to the literature, phenotypes were more severe in *Ywhae*^{-/-} mutants when compared with *Ywhae*^{+/-} mice. With respect to the 3R (replacement, reduction, and refinement) principles to limit animal use, heterozygous *Ywhae*^{tm1e} mutant mice were not studied because our main goal was to gain insights into the in vivo consequences of *YWHAE* full inactivation. In our previous research, *Ywhae*^{tm1e/tm1e} mice showed reduced body weight from weaning age at all time points until 16 weeks of age (Figure 3A adapted from¹⁵). The area under the curve was 22% lower in *Ywhae*^{tm1e/tm1e} compared with WT animals ($P < .05$, t test). At 12 weeks, these differences were mostly driven by a reduction in body length and lean body mass (-8% , $P < 5 \times 10^{-5}$ and -15% , $P < 5 \times 10^{-3}$, respectively) (Figure 3B and C). To determine if these growth delays might also occur during embryogenesis, we assessed embryo morphology in a group of 13 homozygous embryos of the 44 collected. We found that 23% (3 of 13) exhibited embryonic growth retardation, 38.5% (5 of 13) presented with a fetal edema, and 31% (4 of 13) displayed a pale yolk sack (data not shown), suggesting that growth delays originate from embryonic stages.

Food consumption was measured over 21 hours in metabolic cages, and *Ywhae*^{tm1e/tm1e} mice displayed a reduced latency to feeding initiation (Figure 3D). Water intake, however, was normal (data not shown). After 5 hours, the cumulative food intake resumed with similar increments compared with WT, highlighting that the earlier increase in food intake could be the result of hyperactivity, which has been reported before.^{12,13} Thus, the trend toward increase in food consumption does not mirror fat mass (Figure 3E) or fat percentage ($24.4\% \pm 2.5$ vs $21\% \pm 3.2$ in WT and *Ywhae*^{tm1e/tm1e}, respectively), which were identical in both genotypes. Instead, body length and lean mass were significantly reduced (-8% , $P < 10^{-4}$ and -16% , $P < .005$, respectively), highlighting growth delay. Indirect calorimetric analysis in individual cages highlighted hyperactivity at night (Supplemental Figure 1 and Supplemental Table 1). The respiratory exchange ratio was slightly elevated in *Ywhae*^{tm1e/tm1e} mice, indicative of greater use of carbohydrates as a substrate, and could again be correlated to hyperactivity because this feature was only present for low respiratory exchange ratio readings and only during the first 5 hours of the acclimatization period (Supplemental Figure 1). This suggests that physical alterations in *Ywhae*^{tm1e/tm1e} mice result from developmental abnormalities rather than a metabolic origin. Standard measures of plasma metabolites showed an increase in sodium (+2%), glycerol (+48%), alkaline phosphatase (+41%), and aspartate aminotransferase (+42%) (Supplemental Table 2). Hematology profiles showed increased white and red blood cell counts (+48% and +12%, respectively) (Supplemental Table 3). Bone area and mineral content showed a reduction (-19.2% , $P < 10^{-6}$ and -22.9% , $P < 10^{-4}$, respectively), whereas bone density was not affected (not significant) (Figure 3F-H). Except for a shortened skull and a concave nasal spline, the bone shape and morphology assessed by radiography (Supplemental Table 4) and other variables, such as coat and skin color, head size and morphology, fore- and hindlimb size and morphology, digit fusion, and nail counts, were normal in *Ywhae*^{tm1e/tm1e} mice.

A previous study reported an abnormal morphology of the hippocampus when *Ywhae* is inactivated in the mouse.¹⁰ In this study, comprehensive neuroanatomical phenotyping of adult and embryos in *Ywhae*^{tm1e/tm1e} mice allowed us to find new features relevant to human *YWHAE* variants that have not been reported before.

Among the 22 brain parameters assessed at Bregma +0.98 mm, severe and multiple brain defects, including microcephaly, were identified in male *Ywhae*^{tm1e/tm1e} mice and are summarized in Figure 3I and J. The total brain area at Bregma +0.98 mm was reduced (-18% , $P = .02$). Strikingly, mutant mice showed a compression of the genu of the corpus callosum width (-67% , $P = 10^{-5}$) associated with enlarged lateral ventricles ($+394\%$ on average, $P < 10^{-4}$) (Figure 3K). In addition, we observed an unusual mass of axons ventrally contiguous to the midline of the corpus callosum (black arrow, Figure 3K) that could potentially originate from dysregulation in the navigation of postcrossing axons in the corpus callosum as previously described.³¹ Fronto-medio-dorsal

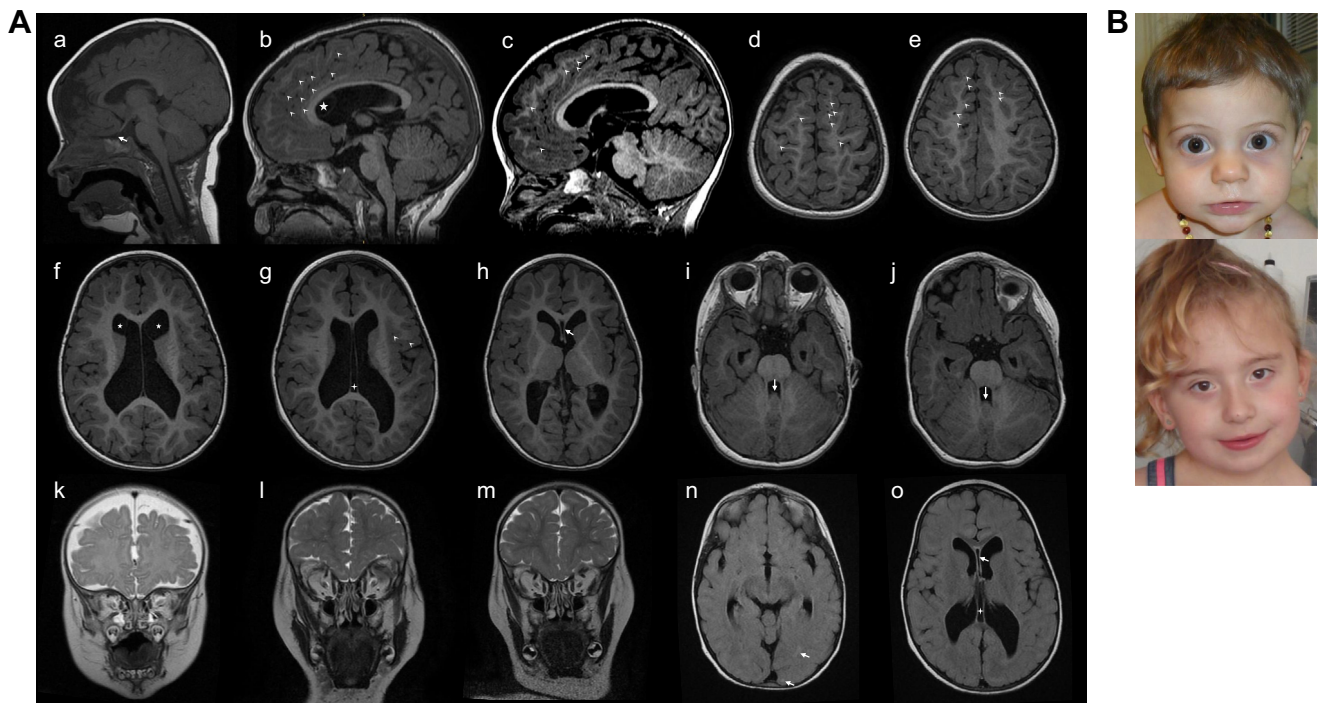


Figure 2 Brain MRIs and photographs in patients. A. Brain MRI images of cases 1 (at 6 months old), 2, and 3 (at 3 years old). (a-c) T1-weighted sagittal brain MRI. (a) Case 1: pituitary hypoplasia (arrow). (b) Case 2: ventricular dilatation, enlarged Virchow-Robin spaces (arrowheads), germinolytic cysts (star), and thin corpus callosum. (c) Case 3: ventricular dilatation, enlarged Virchow-Robin spaces (arrowheads), and thin corpus callosum. (d-j) T1-weighted axial brain MRI. (d) Case 2: enlarged Virchow-Robin spaces (arrowheads). (e) Case 3: enlarged Virchow-Robin spaces (arrowheads). (f) Case 2: ventricular dilatation and germinolytic cysts (star). (g) Case 3: ventricular dilatation and septum pellucidum cyst (cross). (h) Case 3: ventricular dilatation and cavum vergae cyst (arrow). (i) Case 2: cerebellar vermis hypoplasia (arrow). (j) Case 3: cerebellar vermis hypoplasia (arrow). (k) T2 weighted coronal brain MRI in case 1: presence of the olfactory bulbs. (l) T2 Fast recovery fast spin echo weighted coronal brain MRI in case 2: absence of the olfactory bulbs. (m) T2 Fast spin echo weighted coronal brain MRI in case 3: absence of the olfactory bulbs. (n-o) T2 Fluid-attenuated inversion recovery weighted axial brain MRI. (n) Case 2: isointense white matter, with loss of gray/white dedifferentiation and hypersignal of the posterior white matter showing delayed myelination with age (arrow). (o) Case 3: isointense white matter, with loss of gray/white dedifferentiation showing delayed myelination with age, ventricular dilatation, septum pellucidum (cross), and cavum vergae cysts (arrow). B. Photographs of cases 4 and 10 from top to bottom. *MRI*, magnetic resonance imaging.

cortical areas were also reduced in size with the cingulate cortex area, width, and height all being significantly affected ($P < .05$). Interestingly, white matter structures were also reduced in size independently of local pressure from other parameters. This was the case for the anterior commissure (-43% , $P < 10^{-4}$), which is situated on the floor of the caudate putamen (not significant). Basic neurologic assessment did not reveal any gross abnormalities (Supplemental Table 5), although not every neurologic function was tested because it has been extensively published elsewhere.¹³ To discriminate congenital brain malformations from acquired brain abnormalities (when the brain is normal at birth but shows abnormalities subsequently), we studied brain morphology at embryonic day 14.5 (E14.5) using HREM datasets (Figure 3L). More specifically, we reassessed phenotypes present in adults using the murine developmental brain atlas³² and online software available through the Deciphering the Mechanisms of Developmental Disorders consortium website. Lateral ventricle enlargement was clearly

visible on parasagittal planes, whereas thinning of cortical layers (cortical plate and cortical subventricular layer) was also evident on coronal sections (black arrows, Figure 3L). Together, these results indicate that neuroanatomical defects pertaining to ventricles, white matter structures, and brain size originate early during embryonic life.

Discussion

Here, we report clinical manifestations of 15 patients with clear dose-dependent loss-of-function variants in *YWHAE*, 5 of which are patients with variants affecting only *YWHAE* showing developmental and speech delays (5 of 5) as well as brain malformations (4 of 4), establishing *YWHAE* as a gene causing a rare neurodevelopmental disease. Splice variants were carried by 3 of the 15 patients, whereas 12 of 15 had deletions encompassing the *YWHAE* gene (2 small

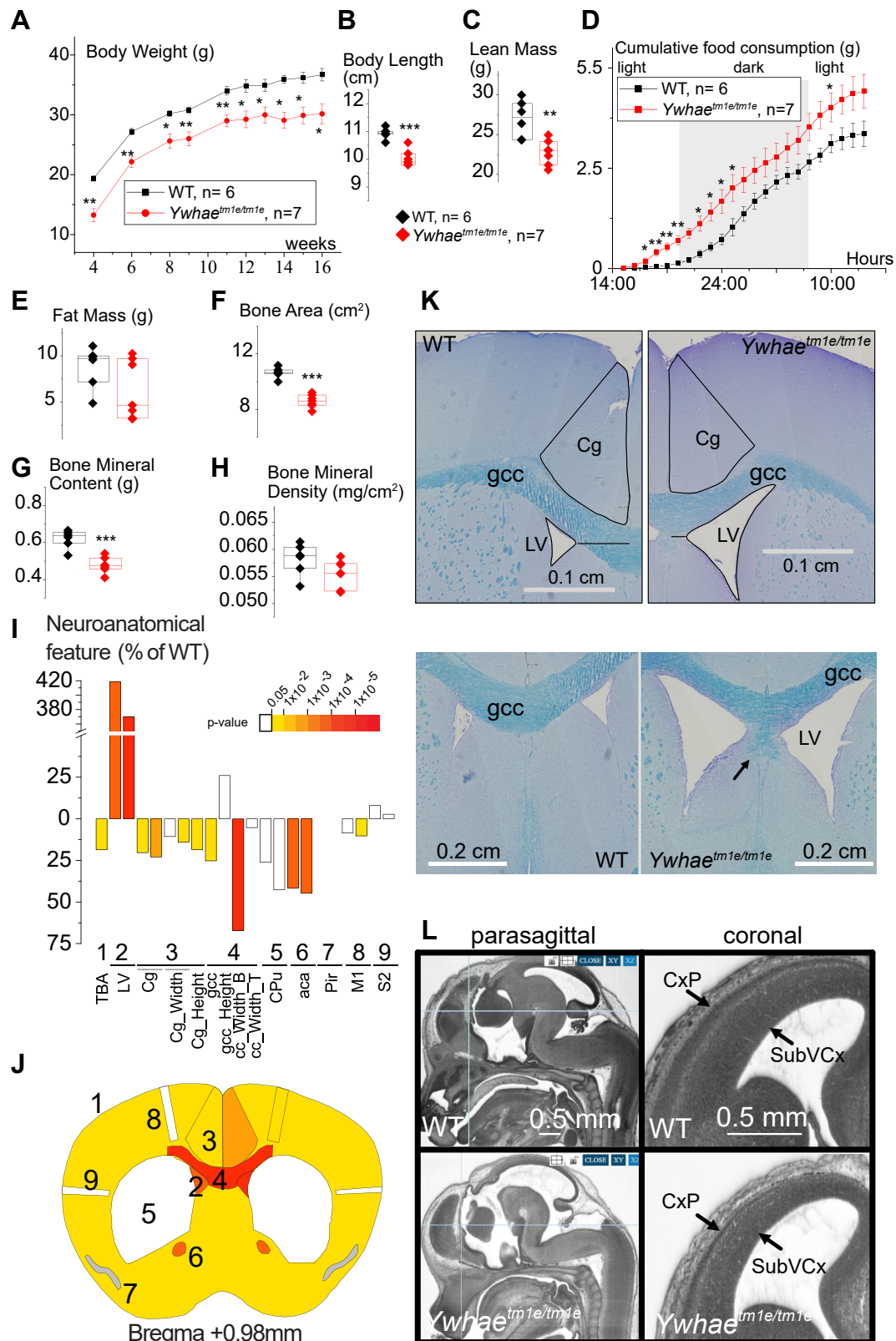


Figure 3 *Ywhae^{tm1e/tm1e}* mice display an array of developmental and neuroanatomical phenotypes. A. Body weight in *Ywhae^{tm1e/tm1e}* male mice from 4 to 16 weeks (data from Ingham et al¹⁵). B, C. Body length and mean mass. D. Cumulative food consumption over 21 hours measured in calorimetric cages. E. Fat mass at 14 weeks. F-H. Bone area, mineral content, and density (14 weeks). I. Histogram with fold increase/decrease expressed as percentage of wild-type mice. Plain lines regroup parameters or left and right hemispheres. Dotted lines indicate left and right hemispheres. Colored regions indicate the presence of at least one significant parameter within the brain region at the 0.05 level. J. Schematic representation of affected brain regions in mice plotted in coronal planes (Bregma +0.98 mm) according to *P* values.

intragenic deletions predicted to cause a frameshift and 10 larger deletions encompassing additional genes in 17p13.3). When the inheritance was known, variants occurred de novo with the exception of 2 variants inherited from a symptomatic parent or a healthy mosaic father.

We did not identify any recurrent variant—except for the one present in the 2 monozygotic twins—nor did we identify pathogenic nonsense, missense, or indel variants in *YWHAE*. Some regions of *YWHAE* present a strong constraint to missense variants because they do not seem to tolerate any such variant (gnomAD v2.1.1).³³ Although we only identified loss-of-function variants in *YWHAE*, we do not exclude the possibility that missense variants could also alter 14-3-3 ϵ protein function. It is noteworthy that the Decipher (ID 359873 and 288974) and ClinVar (VCV000148756 and VCV000154956) databases show 4 additional deletions of *YWHAE* alone, one of which (VCV000154956) is located in coding regions, reported in an individual with autistic behavior. No further clinical details and inheritance information are provided on these online databases, although autism is known to be associated with disorders of the corpus callosum.³⁴

We are aware of only 1 case reported in the literature with a deletion of *YWHAE* alone.⁶ We identified 4 additional individuals with *YWHAE* variants alone bringing the total number of patients with specific variants in *YWHAE* to 5. This allowed a better delineation of the core phenotypes associated specifically with *YWHAE* loss of function, which consistently included global developmental delay with impaired language, hypotonia, and brain malformations, including corpus callosum hypoplasia, delayed myelination, and ventricular dilatation (see Table 1 for a summary or Table 2 for a detailed phenotypic description). We found notable neuroanatomical phenotypic overlap with homozygous *Ywhae*^{tm1e/tm1e} mutant mice, which displayed multiple brain structure defects, including hydrocephaly, dysgenesis of the corpus callosum, small anterior commissure, and thin motor and cingulate cortices, present before birth. The novelty of our murine findings in the context of previous *Ywhae* mouse reports^{9,10,12-15} lies in the comprehensive assessment of neuroanatomical phenotypes relying on a newly developed precision histology approach,²⁴ allowing us to detect more subtle neuroanatomical differences (see Figure 3K for an example).

Seizures and behavioral abnormalities were commonly present in patients (see Table 1). Dysmorphic facial features seem to be milder when compared with individuals with

deletion encompassing more than just *YWHAE*. Only 1 of 5 patients presented with mild ID. Cases with a variant specifically in *YWHAE* did not show growth retardation in contrast to patients with more than 1 gene affected, which included the *CRK* gene previously reported to be associated with growth retardation in the MDS.²⁹ Intriguingly, *Ywhae*^{tm1e/tm1e} mice exhibited a reduced body weight in line with previous knockout mouse studies on different genetic backgrounds.^{10,13,15} No gross behavioral abnormalities using the modified SHIRPA procedure²⁰ were seen in our mice and epilepsy was not modeled. However, in a previous study dedicated to neurocognitive behaviors in *Ywhae* homozygous knockouts, mice showed increased locomotor activity and deficits in cognition.¹³

Although the precise molecular role of 14-3-3 ϵ in the development of the corpus callosum remains unclear, it has been shown that 14-3-3 proteins regulate the switch from sonic hedgehog-mediated commissural axon attraction to repulsion after midline crossing in the developing mouse spinal cord.³⁵ The involvement of 14-3-3 ϵ in a switch that controls repulsive guidance clues was further evidenced in motor axons derived from the fruit fly CNS model system.³⁶ It is thus tempting to speculate that the mass of axons we detected beneath the corpus callosum (black arrow, Figure 3K) may be due to misregulation of commissural axon attraction and repulsion, potentially caused by the absence of 14-3-3 ϵ . Through its interactions with LIS1 and NUDEL, 14-3-3 ϵ is also known to interact with dynein. When 14-3-3 ϵ is deficient in mice, there is a reduction in cytoplasmic dynein function, thereby underlining its role in neuronal migration.^{10,37} Via its interactions with dynein, it could be hypothesized that loss of 14-3-3 ϵ could affect corticogenesis and explain the thinning of the motor and cingulate cortices in mice. However, further analyses should be performed to study the precise function of 14-3-3 ϵ protein in corticogenesis and colossal axon crossing at the midline.

Conclusion

To our knowledge, this study presents the first molecular and clinical description of a rare neurodevelopmental disorder occurring with brain abnormalities caused by heterozygous loss-of-function SNVs in *YWHAE* and gathers new or previously reported cases with deletion encompassing *YWHAE* but not *PAFAH1B1*. Moreover, studies of *Ywhae*^{tm1e/tm1e} mice showed neuroanatomical defects

The color map indicates *P* value below the threshold of .05 or gray in which the *n* was too low to calculate statistics. K. Nissl-stained coronal brain sections from WT and *Ywhae*^{tm1e/tm1e} mice, showing the reduction of the cingulate cortex, the reduction of the width of the genu of the corpus callosum, the enlargement of the lateral ventricles, and an unusual mass of axons beneath the genu of the corpus callosum at the midline (black arrow). L. HREM analysis of 14.5 embryos showing on the left, enlarged ventricle (parasagittal sections) and on the right panel, the thinning of the cortical plate and subventricular layer cortex (coronal sections). The vertical blue lines on the parasagittal section (left) indicate the corresponding coronal plane (shown on right panel), whereas the horizontal blue lines indicate the corresponding longitudinal plane (not shown) using ImageJ plugins. *Aca*, anterior commissure; *cc*, corpus callosum; *Cg*, cingulate cortex; *CPu*, caudate putamen; *CxP*, cortical plate; *gcc*, genu of the corpus callosum; *HREM*, high-resolution episcopic microscopy; *LV*, lateral ventricle; *MI*, primary motor cortex; *Pir*, piriform cortex; *S2*, second somatosensory cortex; *SubVCx*, subventricular layer cortex; *TBA*, total brain area; *WT*, wild-type.

similar to those seen in the human condition, reinforcing the importance of *YWHAE* in the proper development of the mammalian brain.

Together, these results suggest that *YWHAE* loss of function results in a neurodevelopmental syndrome with brain abnormalities involving corpus callosum dysgenesis with milder phenotypes than the contiguous gene deletion syndrome of chromosome 17p13.3 without the *PAFAH1B1* deletion.

To improve the identification and management of this new syndrome, the clinical data would need to be enriched, in particular with respect to the neurocognitive profile and the long-term outcome of these patients.

Data Availability

The datasets generated during this study are available upon request from the corresponding authors.

Acknowledgments

We thank the families for taking part in the study. We thank the CCuB for technical support and management of the computing platform. We thank ERN-ITHACA and the GeneMatcher platform for data sharing. Several authors are members of ERN-ITHACA. We acknowledge Christophe Ouzouf, Jérémie Roquet, Mathieu Chopelet, and Laura Fenlon for discussion or providing comments on the manuscript. We thank the members of the Sanger Institute Mouse Pipelines teams and the Research Support Facility for the provision and management of the *Ywhae*^{tm1e/tm1e} knockout mice.

Funding

This work was supported by grants from the French National Institute of Health and Medical Research (First Step to BY), the French National Research Agency (ANR JCJC to BY), the European Union through the FEDER program (to GAD), and by the Wellcome Trust Grant 206194. The Deciphering the Mechanisms of Developmental Disorders (DMDD) program was funded by the Wellcome Trust (Grant 100160) with support from the Francis Crick Institute, licensed under a Creative Commons Attribution license (CC BY 4.0). The funders had no role in study design, data collection and analysis, decision to publish, or preparation of the manuscript.

Author Information

Data curation: A.-S.D.-P., V.E.V., J.A.R., C.J.L.; Investigation: A.-S.D.-P., S.C.C., A.-L.B., A.M., C.W., V.E.V.,

C.E.P., M.P.-B., F.S.-S., M.P.-M., T.B., E.L., C.A.B., J.A.R., M.E., M.A.M., J.L., B.D., C.J.L.; Resources: V.E.V., C.J.L.; Software: Y.D.; Supervision: A.-S.D.-P., L.F., B.Y.; Writing-original draft: A.-S.D.-P., S.C.C., B.Y.; Writing-review and editing: A.-S.D.-P., A.-L.B., V.E.V., Q.T., C.E.P., E.L., J.A.R., C.P., L.F., B.Y.

Ethics Declaration

This study conforms to the Helsinki Declaration of ethical principles for medical research involving human subjects. When additional analyses not included in the care approach were required (RNA studies), they were done in the framework of the DISCOVERY project, which was approved by the appropriate French independent ethics committee (Comité de Protection des Personnes 2016-A01347-44), and samples were part of the GAD collection DC2011-1332. The care and use of mice were in accordance with the UK Home Office regulations, UK Animals (Scientific Procedures) Act of 1986. Permission was obtained to publish photographs of cases 4 and 10.


Conflict of interest

The authors declare no conflicts of interest.

Additional Information

The online version of this article (<https://doi.org/10.1016/j.gim.2023.100835>) contains supplementary material, which is available to authorized users.

Authors

Anne-Sophie Denommé-Pichon^{1,2,3,*} ,
Stephan C. Collins², Ange-Line Bruel^{1,2}, Anna Mikhaleva⁴,
Christel Wagner⁵, Valerie E. Vancollie⁶,
Quentin Thomas^{2,7}, Martin Chevarin^{1,2}, Mathys Weber^{2,8},
Carlos E. Prada⁹, Alexis Overs^{1,2},
María Palomares-Bralo^{3,10,11},
Fernando Santos-Simarro^{3,10,11}, Marta Pacio-Míguez¹¹,
Tiffany Busa¹², Eric Legius¹³, Carlos A. Bacino¹⁴,
Jill A. Rosenfeld^{14,15}, Gwenaël Le Guyader¹⁶,
Matthieu Egloff^{16,17}, Xavier Le Guillou¹⁶,
Maria Antonietta Mencarelli¹⁸, Alessandra Renieri^{18,19,20},
Salvatore Grosso^{21,22}, Jonathan Levy²³,
Blandine Dozières²⁴, Isabelle Desguerre²⁵,
Antonio Vitobello^{1,2,3}, Yannis Duffourd^{1,2},
Christopher J. Lelliott⁶, Christel Thauvin-Robinet^{1,2,8},
Christophe Philippe^{1,2}, Laurence Faivre^{2,3,8},
Binnaz Yalcin^{2,*}

Affiliations

¹Functional Unit for Diagnostic Innovation in Rare Diseases, FHU-TRANSLAD, Dijon Bourgogne University Hospital, Dijon, France; ²UMR1231 GAD “Génétique des Anomalies du Développement”, INSERM, FHU-TRANSLAD, University of Burgundy, Dijon, France; ³European Reference Network, ERN-ITHACA; ⁴Center for Integrative Genomics, University of Lausanne, Lausanne, Switzerland; ⁵UMR7104, U964, INSERM, IGBMC, Illkirch, France; ⁶Wellcome Sanger Institute, Hinxton, Cambridge, United Kingdom; ⁸Department of Genetics and Reference Center for Development Disorders and Intellectual Disabilities, FHU-TRANSLAD and GIMI Institute, Dijon Bourgogne University Hospital, Dijon, France; ⁷Department of Neurology, Dijon Bourgogne University Hospital, Dijon, France; ⁹Division of Genetics, Birth Defects & Metabolism, Ann & Robert H. Lurie Children's Hospital of Chicago, Chicago, IL; ¹⁰Institute of Medical and Molecular Genetics (INGEMM), La Paz University Hospital, Autonomous University of Madrid, IdiPAZ, Madrid, Spain; ¹¹Rare Diseases Networking Biomedical Research Centre (CIBERER), Carlos III Institute, Madrid, Spain; ¹²Department of Medical Genetics, CHU Timone Enfants, AP-HM, Marseille, France; ¹³Laboratory for Neurofibromatosis Research, Department of Human Genetics, KU Leuven University Hospital, Belgium; ¹⁴Department of Molecular and Human Genetics, Baylor College of Medicine, Houston, TX; ¹⁵Baylor Genetics Laboratories, Houston, TX; ¹⁶Genetics Department, Poitiers University Hospital, Poitiers, France; University of Poitiers, Poitiers, France; ¹⁷Experimental and Clinical Neurosciences Laboratory, INSERM, University of Poitiers, Poitiers, France; ¹⁸Medical Genetics, Azienda Ospedaliero-Universitaria Senese, Siena, Italy; ¹⁹Medical Genetics, University of Siena, Siena, Italy; ²⁰Med Biotech Hub and Competence Center, Department of Medical Biotechnologies, University of Siena, Siena, Italy; ²¹Department of Molecular and Developmental Medicine, University of Siena, Siena, Italy; ²²U.O.C. Pediatria, Azienda Ospedaliera Universitaria Senese, Siena, Italy; ²³Genetics Department, Robert-Debré University Hospital, APHP, Paris, France; ²⁴Department of Pediatric Neurology and Metabolic Diseases, Robert Debré University Hospital, APHP, Paris, France; ²⁵Departments of Pediatric Neurology and Medical Genetics, Hôpital Necker-Enfants Malades, Université Paris Cité, Paris, France

References

- Chong SS, Pack SD, Roschke AV, et al. A revision of the lissencephaly and Miller-Dieker syndrome critical regions in chromosome 17p13.3. *Hum Mol Genet.* 1997;6(2):147-155. <http://doi.org/10.1093/hmg/6.2.147>
- Dobyns WB, Curry CJ, Hoyme HE, Turlington L, Ledbetter DH. Clinical and molecular diagnosis of Miller-Dieker syndrome. *Am J Hum Genet.* 1991;48(3):584-594.
- Ledbetter SA, Kuwano A, Dobyns WB, Ledbetter DH. Microdeletions of chromosome 17p13 as a cause of isolated lissencephaly. *Am J Hum Genet.* 1992;50(1):182-189.
- Jones KL, Gilbert EF, Kaveggia EG, Opitz JM. The Miller-Dieker syndrome. *Pediatrics.* 1980;66(2):277-281. <http://doi.org/10.1542/peds.66.2.277>
- Cardoso C, Leventer RJ, Ward HL, et al. Refinement of a 400-kb critical region allows genotypic differentiation between isolated lissencephaly, Miller-Dieker syndrome, and other phenotypes secondary to deletions of 17p13.3. *Am J Hum Genet.* 2003;72(4):918-930. <http://doi.org/10.1086/374320>
- Noor A, Bogatan S, Watkins N, Meschino WS, Stavropoulos DJ. Disruption of YWHAE gene at 17p13.3 causes learning disabilities and brain abnormalities. *Clin Genet.* 2018;93(2):365-367. <http://doi.org/10.1111/cge.13056>
- Berg D, Holzmann C, Riess O. 14-3-3 proteins in the nervous system. *Nat Rev Neurosci.* 2003;4(9):752-762. <http://doi.org/10.1038/nrn1197>
- Li Q, Cheng Z, Zhou L, et al. Developmental heterogeneity of microglia and brain myeloid cells revealed by deep single-cell RNA sequencing. *Neuron.* 2019;101(2):207-223.e10. <http://doi.org/10.1016/j.neuron.2018.12.006>
- Cornell B, Wachi T, Zhukarev V, Toyo-oka K. Regulation of neuronal morphogenesis by 14-3-3epsilon (Ywhae) via the microtubule binding protein, doublecortin. *Hum Mol Genet.* 2016;25(20):4405-4418. <http://doi.org/10.1093/hmg/ddw270>
- Toyo-oka K, Shionoya A, Gambello MJ, Cardoso C, et al. 14-3-3epsilon is important for neuronal migration by binding to NUDEL: a molecular explanation for Miller-Dieker syndrome. *Nat Genet.* 2003;34(3):274-285. <http://doi.org/10.1038/ng1169>
- Bi W, Sapir T, Shchelochkov OA, et al. Increased LIS1 expression affects human and mouse brain development. *Nat Genet.* 2009;41(2):168-177. <http://doi.org/10.1038/ng.302>
- Ikeda M, Hikita T, Taya S, et al. Identification of YWHAE, a gene encoding 14-3-3epsilon, as a possible susceptibility gene for schizophrenia. *Hum Mol Genet.* 2008;17(20):3212-3222. <http://doi.org/10.1093/hmg/ddn217>
- Wachi T, Cornell B, Toyo-Oka K. Complete ablation of the 14-3-3epsilon protein results in multiple defects in neuropsychiatric behaviors. *Behav Brain Res.* 2017;319:31-36. <http://doi.org/10.1016/j.bbr.2016.11.016>
- Toyo-oka K, Wachi T, Hunt RF, et al. 14-3-3ε and ζ regulate neurogenesis and differentiation of neuronal progenitor cells in the developing brain. *J Neurosci.* 2014;34(36):12168-12181.
- Ingham NJ, Pearson SA, Vancollie VE, et al. Mouse screen reveals multiple new genes underlying mouse and human hearing loss. *PLoS Biol.* 2019;17(4):e3000194. <http://doi.org/10.1371/journal.pbio.3000194>
- Sobreira N, Schiettecatte F, Valle D, Hamosh A. GeneMatcher: a matching tool for connecting investigators with an interest in the same gene. *Hum Mutat.* 2015;36(10):928-930. <http://doi.org/10.1002/humu.22844>
- Richards S, Aziz N, Bale S, et al. Standards and guidelines for the interpretation of sequence variants: a joint consensus recommendation of the American College of Medical Genetics and Genomics and the Association for Molecular Pathology. *Genet Med.* 2015;17(5):405-424. <http://doi.org/10.1038/gim.2015.30>
- Skarnes WC, Rosen B, West AP, et al. A conditional knockout resource for the genome-wide study of mouse gene function. *Nature.* 2011;474(7351):337-342. <http://doi.org/10.1038/nature10163>
- Ryder E, Gleeson D, Sethi D, et al. Molecular characterization of mutant mouse strains generated from the EUCCOMM/KOMP-CSD ES

- cell resource. *Mamm Genome*. 2013;24(7-8):286-294. <http://doi.org/10.1007/s00335-013-9467-x>
20. White JK, Gerdin AK, Karp NA, et al. Genome-wide generation and systematic phenotyping of knockout mice reveals new roles for many genes. *Cell*. 2013;154(2):452-464. <http://doi.org/10.1016/j.cell.2013.06.022>
21. Mikhaleva A, Kannan M, Wagner C, Yalcin B. Histomorphological phenotyping of the adult mouse brain. *Curr Protoc Mouse Biol*. 2016;6(3):307-332. <http://doi.org/10.1002/cpmo.12>
22. Collins SC, Mikhaleva A, Vrcelj K, et al. Large-scale neuroanatomical study uncovers 198 gene associations in mouse brain morphogenesis. *Nat Commun*. 2019;10(1):3465. <http://doi.org/10.1038/s41467-019-11431-2>
23. Weninger WJ, Geyer SH, Mohun TJ, et al. High-resolution episcopic microscopy: a rapid technique for high detailed 3D analysis of gene activity in the context of tissue architecture and morphology. *Anat Embryol (Berl)*. 2006;211(3):213-221. <http://doi.org/10.1007/s00429-005-0073-x>
24. Collins SC, Wagner C, Gagliardi L, et al. A method for parasagittal sectioning for neuroanatomical quantification of brain structures in the adult mouse. *Curr Protoc Mouse Biol*. 2018;8(3):e48. <http://doi.org/10.1002/cpmo.48>
25. Romano C, Ferranti S, Mencarelli MA, Longo I, Renieri A, Grosso S. 17p13.3 microdeletion including YWHAE and CRK genes: towards a clinical characterization. *Neurol Sci*. 2020;41(8):2259-2262. <http://doi.org/10.1007/s10072-020-04424-3>
26. Mignon-Ravix C, Cacciagli P, El-Waly B, et al. Deletion of YWHAE in a patient with periventricular heterotopias and pronounced corpus callosum hypoplasia. *J Med Genet*. 2010;47(2):132-136. <http://doi.org/10.1136/jmg.2009.069112>
27. Chen CP, Ko TM, Wang LK, et al. Prenatal diagnosis of a 0.7-Mb 17p13.3 microdeletion encompassing YWHAE and CRK but not PAFAH1B1 in a fetus without ultrasound abnormalities. *Taiwan J Obstet Gynecol*. 2018;57(1):128-132. <http://doi.org/10.1016/j.tjog.2017.12.022>
28. Schiff M, Delahaye A, Andrieux J, et al. Further delineation of the 17p13.3 microdeletion involving YWHAE but distal to PAFAH1B1: four additional patients. *Eur J Med Genet*. 2010;53(5):303-308. <http://doi.org/10.1016/j.ejmg.2010.06.009>
29. Nagamani SCS, Zhang F, Shchelochkov OA, et al. Microdeletions including YWHAE in the Miller-Dieker syndrome region on chromosome 17p13.3 result in facial dysmorphisms, growth restriction, and cognitive impairment. *J Med Genet*. 2009;46(12):825-833. <http://doi.org/10.1136/jmg.2009.067637>
30. Bruno DL, Anderlid BM, Lindstrand A, et al. Further molecular and clinical delineation of co-locating 17p13.3 microdeletions and microduplications that show distinctive phenotypes. *J Med Genet*. 2010;47(5):299-311. <http://doi.org/10.1136/jmg.2009.069906>
31. Mire E, Hocine M, Bazellières E, et al. Developmental upregulation of Ephrin-B1 silences Sema3C/Neuropilin-1 signaling during post-crossing navigation of corpus callosum axons. *Curr Biol CB*. 2018;28(11):1768-1782.e4. <http://doi.org/10.1016/j.cub.2018.04.026>
32. Paxinos G, Halliday GM, Watson C, Koutcherov Y, Wang H. *Atlas of the Developing Mouse Brain at E17.5, P0 and P6*. Cambridge: Academic Press; 2007.
33. Karczewski KJ, Francioli LC, Tiao G, et al. The mutational constraint spectrum quantified from variation in 141,456 humans. *Nature*. 2020;581(7809):434-443. <http://doi.org/10.1038/s41586-020-2308-7>
34. Paul LK, Corsello C, Kennedy DP, Adolphs R. Agenesis of the corpus callosum and autism: a comprehensive comparison. *Brain*. 2014;137(6):1813-1829. <http://doi.org/10.1093/brain/awu070>
35. Yam PT, Kent CB, Morin S, et al. 14-3-3 proteins regulate a cell-intrinsic switch from sonic hedgehog-mediated commissural axon attraction to repulsion after midline crossing. *Neuron*. 2012;76(4):735-749. <http://doi.org/10.1016/j.neuron.2012.09.017>
36. Yang T, Terman JR. 14-3-3ε couples protein kinase A to semaphorin signaling and silences plexin rasgap-mediated axonal repulsion. *Neuron*. 2012;74(1):108-121. <http://doi.org/10.1016/j.neuron.2011.12.034>
37. Moon HM, Wynshaw-Boris A. Cytoskeleton in action: lissencephaly, a neuronal migration disorder. *Wiley Interdiscip Rev Dev Biol*. 2013;2(2):229-245. <http://doi.org/10.1002/wdev.67>
38. Kent WJ, Sugnet CW, Furey TS, et al. The human genome browser at UCSC. *Genome Res*. 2002;12(6):996-1006. <http://doi.org/10.1101/gr.229102>